DOI: 10.1002/adma.200800295

Fabrication and Characterization of Ultrahigh-Volume-Fraction Aligned Carbon Nanotube–Polymer Composites**

By *Brian L. Wardle,** *Diego S. Saito, Enrique J. García, A. John Hart, Roberto Guzmán de Villoria,* and *Eric A. Verploegen*

High-volume-fraction aligned carbon nanotube (CNT) nanocomposites are envisioned as a revolutionary advanced composite material for a host of demanding applications. A method is described to fabricate such nanocomposites using mechanical densification of vertically aligned CNT forests followed by capillarity-induced wetting with unmodified complex thermosets, including aerospace-grade epoxies. We demonstrate that aligned nanocomposites can be fabricated to high (up to 22%) volume fractions, approaching posited theoretical limits where inter-CNT spacing approaches characteristic lengths of the polymer chains. Scanning electron microscopy (SEM) and X-ray scattering reveal that CNT alignment and distribution are maintained in the nanocomposites. No evidence is found of polymer morphology changes due to the closely-packed CNTs in wide-angle X-ray scattering studies. Variable control of volume fraction with the method demonstrated here produces well-controlled millimeter-scale aligned-CNT nanocomposites that can be used to assess multifunctional properties of these aligned ''fiber'' composites, and investigate nanoscale interactions between the constituents in a controlled manner.

Since their identification,[1,2] carbon nanotubes (CNTs) have captured the imagination of society as much as engineers and scientists.[3,4] At small scales, and for pristine CNTs, CNT properties are unrivaled by any other material, especially when the properties are normalized to density, for example, specific stiffness, modulus over density (E/ρ). CNTs are envisioned as a constituent in numerous applications, particularly as reinforcement in advanced structural composites, owing to their numerous and attractive multifunctional (i.e., mechanical and nonmechanical) properties. However, it has proven difficult to realize the attractive properties of CNTs at engineering-relevant lengthscales owing to synthesis/fabrication issues.[5–8]

Similar to existing advanced-fiber composites, the ideal morphology nanocomposite (NC) has a high volume fraction (V_f) of aligned, collinear, *continuous*, high-quality CNTs homogeneously dispersed in a surrounding matrix without voids or inclusions: an aligned-CNT NC, or A-CNT NC. Predictions of the performance of such a composite have motivated much research,[5,9] including interest in an isotropic (direction-dependent) properties that result from the CNT alignment, for example, a direct application for such structures is as heat sinks in microprocessors.[10] High CNT volume fraction allows the properties of the CNTs to dominate the composite properties, while the matrix provides support (e.g., resisting buckling under shear or compression), protection, and a path for load-sharing between the CNTs. The millimeter-scale nanocomposites synthesized and characterized herein approach the ideal morphology desired for many applications; that of aligned CNTs dispersed uniformly in a polymer matrix. By mechanically densifying an as-grown aligned CNT forest (1% volume fraction), variable control of CNT volume fraction is easily obtained. Combined with polymer infusion into the CNT forests via simple capillarity-driven wetting along the axis of the CNTs, nanocomposites are formed. The process developed (Fig. 1A) allows millimeter-scale A-CNT NC specimens (Fig. 1B) to be fabricated with ultrahigh (approaching practical and theoretical limits) CNT volume fraction. Importantly, the method allows a continuum of volume fractions to be obtained by simply varying the degree of mechanical densification.

Prior work has focused on embedding or mixing short unaligned CNTs in a polymer matrix (usually a thermoplastic in solvent to reduce viscosity and promote CNT dispersion)[5–8,11–15] with much less work on aligned CNT NCs, and none on the ideal morphology beyond theoretical predictions. One significant approach towards the ideal morphology is the creation of aligned CNT yarns by drawing discontinuous CNTs together either in neat yarns[13,16,17] or impregnated with a

[*] Prof. B. L. Wardle, D. S. Satio, Dr. E. J. García, Dr. A. J. Hart, Dr. R. Guzmán de Villoria, E. A. Verploegen
Departments of Aeronautics and Astronautics and Chemical Engineering
Massachusetts Institute of Technology
77 Massachusetts Avenue, Cambridge, MA 02139 (USA)
E-mail: wardle@mit.edu

[**] This work was supported by Airbus S.A.S., Boeing, Embraer, Lockheed Martin, Saab AB, Spirit AeroSystems, and Textron Inc. through MIT's Nano-Engineered Composite aerospace STructures (NECST) Consortium. The authors gratefully acknowledge Dr. Myounggu Park (Univ. of Michigan), Namiko Yamamoto (MIT), and Hulya Cebeci (MIT) for valuable input into this manuscript. The authors thank John Kane and the entire Technology Laboratory for Advanced Materials and Structures (TELAMS) at MIT for technical support, Richard Schalek at the Center for Nanoscale Systems at Harvard Univ. and Patrick Boisvert at the Center for Materials Science and Engineering at MIT for SEM & TEM imaging assistance, Hexcel Corp. for providing resin, and the staff and facilities of the Cornell High Energy Synchrotron Source (CHESS) which is supported by the National Science Foundation and the National Institutes of Health/ National Institute of General Medical Sciences under award DMR-0225180.

ADVANCED MATERIALS

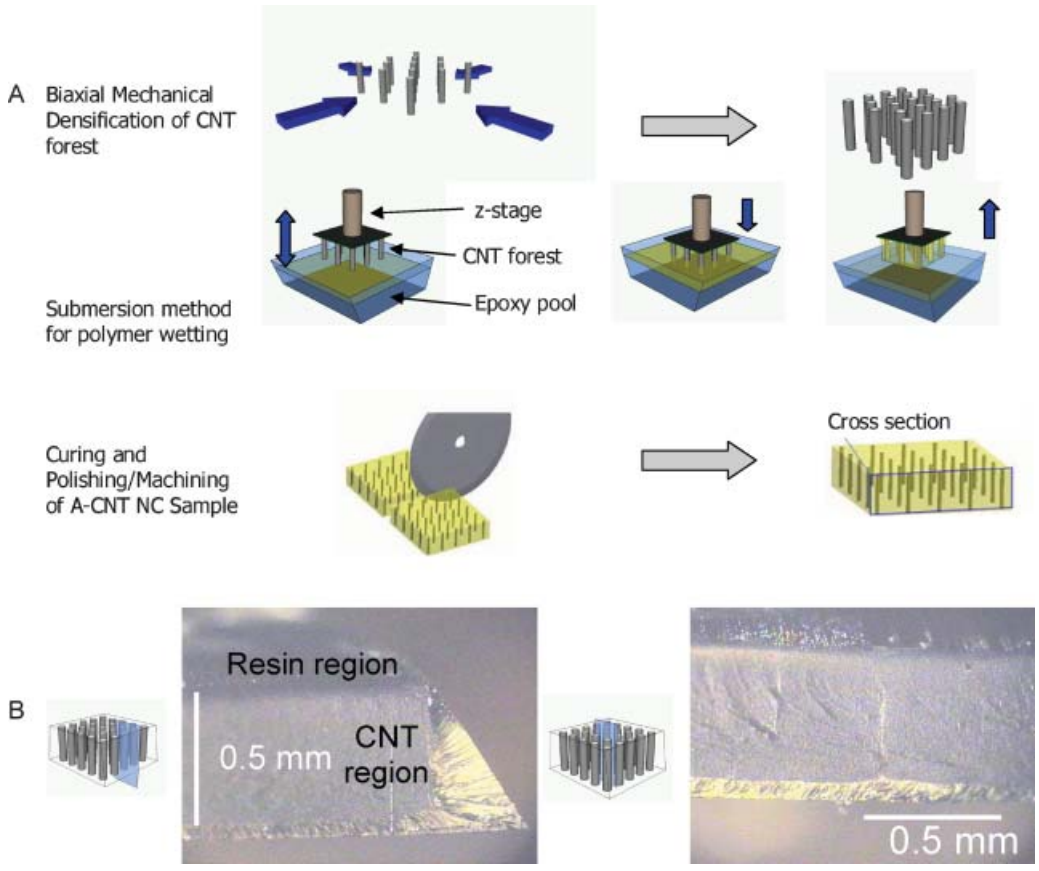

Figure 1. Fabrication of variable volume fraction aligned-CNT nanocomposites. A) Process flow for fabricating nanocomposites. B) Optical images of 1% volume fraction RTM6 nanocomposite specimens after fabrication.

thermoplastic.[18,19] Currently in these yarn processes, the CNTs produce yarns or composites that are discontinuous (CNT lengths to tens of micrometers) and the composites have micrometer-diameter dimensions similar to existing advanced fibers such as carbon. Effects of the discontinuous CNTs on mechanical and transport (electrical, thermal) properties are not known. Another approach for realizing A-CNT NCs is in situ gas-phase polymerization of aligned CNTs[19–22] to create thermoplastic A-CNTs, a process that yields a single as-grown volume fraction and is limited to a small subset of polymers that allow gas-phase polymerization. In situ polymerization would be compatible with the process developed here for variable volume fraction.

Dispersing CNTs in a polymer solution prior to spinning a fiber has resulted in polymeric fibers containing oriented CNTs.[23–26] These fibers have significantly enhanced mechanical properties compared to the pure polymer; however, the structure and properties of these fibers are currently far from the ideal morphology NC. Recently, layer-by-layer assembly has been used to fabricate composite films using nanoclays,[27] as well as films containing CNTs.[28]

In this work, mechanical densification and polymer wetting allow fabrication of the ideal morphology A-CNT NC with thermoset epoxies, including aerospace-grade epoxies used currently in the most advanced composite materials. Three polymers are used to fabricate the A-CNT NCs: 1- and 2-part aerospace-grade epoxies used in resin-transfer molding (RTM) of carbon-fiber advanced composites, and SU-8, a UV-curable thermoset used extensively in microfabrication. Volume fraction is varied using the mechanical densification method, and the resulting NCs characterized by optical, scanning, and transmission electron microscopy, and small- and wide-angle X-ray scattering (SAXS and WAXS) to study alignment, dispersion, voids, and the effect of the closely-packed CNTs on polymer curing.

The process for creating the A-CNT NCs follows the flow in Figure 1A. A-CNT forests are grown to millimeter heights on a Si substrate using a modified chemical vapor deposition (CVD) process.[29] The resulting forests have been characterized previously for alignment, CNT dia. distribution, and spacing. The CNTs have average diameter of 8 nm (2–3 walls), are spaced ca. 80 nm apart, and are continuous as a result of the base-growth process.[30] The as-grown A-CNT volume fraction is 1%, giving a coverage of 10^9–10^{10} CNTs per cm^2. The CNTs are well-aligned, as shown in Figure 2; alignment will be further quantified using SAXS for variable volume fractions. The forests are grown on 1 cm^2 Si substrates, and the forests released using a standard razor blade from the growth substrate. The released forest is placed in a small device that allows mechanical biaxial compression in two orthogonal

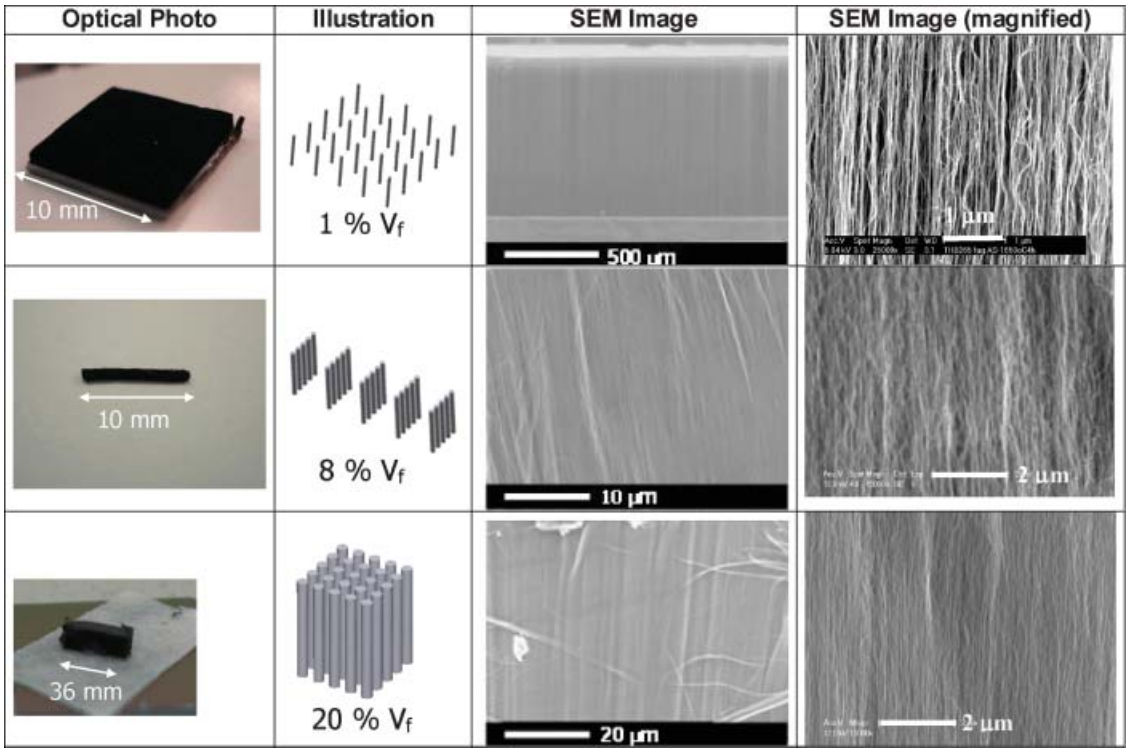

Figure 2. Aligned CNT volume fraction from mechanical densification of ca. 1 mm tall A-CNT forests at 1% (as-grown), 8% (uniaxially densified), and 20% (biaxially densified) volume fraction.

directions. By varying the distance the forest is compressed, variable-density CNT forests are obtained as shown in Figure 2. These (densified) forests are transferred to a z-stage using SEM tape and lowered into a pool of uncured polymer.[31] The polymer pool is heated for the aerospace epoxies to simulate their processing, and SU-8 is similarly heated to mimic prebaking. The matrix infuses into the CNT forest via capillary-induced wetting, at rates that depend on properties of the CNT forest (e.g., volume fraction) and the polymer (e.g., viscosity, contact angle).[32,33] The epoxy is cured following the recommended process for each polymer, yielding the desired nanocomposites (Fig. 1B). It is important to note that in the current study, neither the CNTs nor the thermosets are modified, that is, the CNTs are as-grown and the polymers are as-received (no solvents were utilized). Additional details on the polymers used, and their properties and processing appear in the Experimental section.

After preparing the variable volume fraction A-CNT NCs, they are characterized using optical, scanning, and transmission electron microscopy for dispersion, alignment, and overall morphology (e.g., voids). Samples are mechanically fractured along the CNT axis (see illustrations in Fig. 3) to create surfaces to visualize the NC interior (see example optical fracture surfaces in Fig. 1). Fracture surfaces are utilized, rather than polishing, because it has been found to be more effective to visualize nanocomposites.[34,35] A drawback of the fracture-surface preparation method is that the texture of the surface follows local crack propagations and is only indirectly linked to the actual morphology (this is a typical issue also in thin-film cross-sectional analyses). However, it is possible to discern morphology differences especially at high SEM magnification. Fracture surfaces for a series of increasing volume fraction NCs is presented in Figure 3 for VRM34 resin. The neat resin provides a relatively smooth fracture surface, particularly at higher magnification, and there is a clear difference in the fracture surfaces of the NCs versus the neat resin. Finally, especially at high magnification, differences between low and high volume fraction NC fracture morphologies are also evident. At low magnification, the fracture surface is observed to become more homogeneous with increased CNTs, and at higher magnification, CNT density appears to be increasing. Finally, there are also differences between resins, as can be observed in the 1% A-CNT NCs for VRM34 and RTM6 epoxy in Figure 3. Last, it should be noted that micrometer-scale voids were not observed in the NCs, except when attributed to fabrication or handling issues, typically at the specimen edges. Micrometer-scale polymer regions were observed in some specimens, with a clear trend of reducing these regions at higher CNT volume fractions. Pure polymer regions effectively disappeared at CNT volume fractions greater than ca. 8%. These regions are attributed to the competition between the transverse stiffness of the CNT forest and the compaction forces generated during capillarity-induced wetting. At low CNT volume fraction, the CNT forests contract to a greater degree when wet by polymers than at higher volume fraction. At a certain volume fraction, dependent on CNT and polymer characteristics, the forest stiffness will approximately balance the compaction forces

ADVANCED MATERIALS

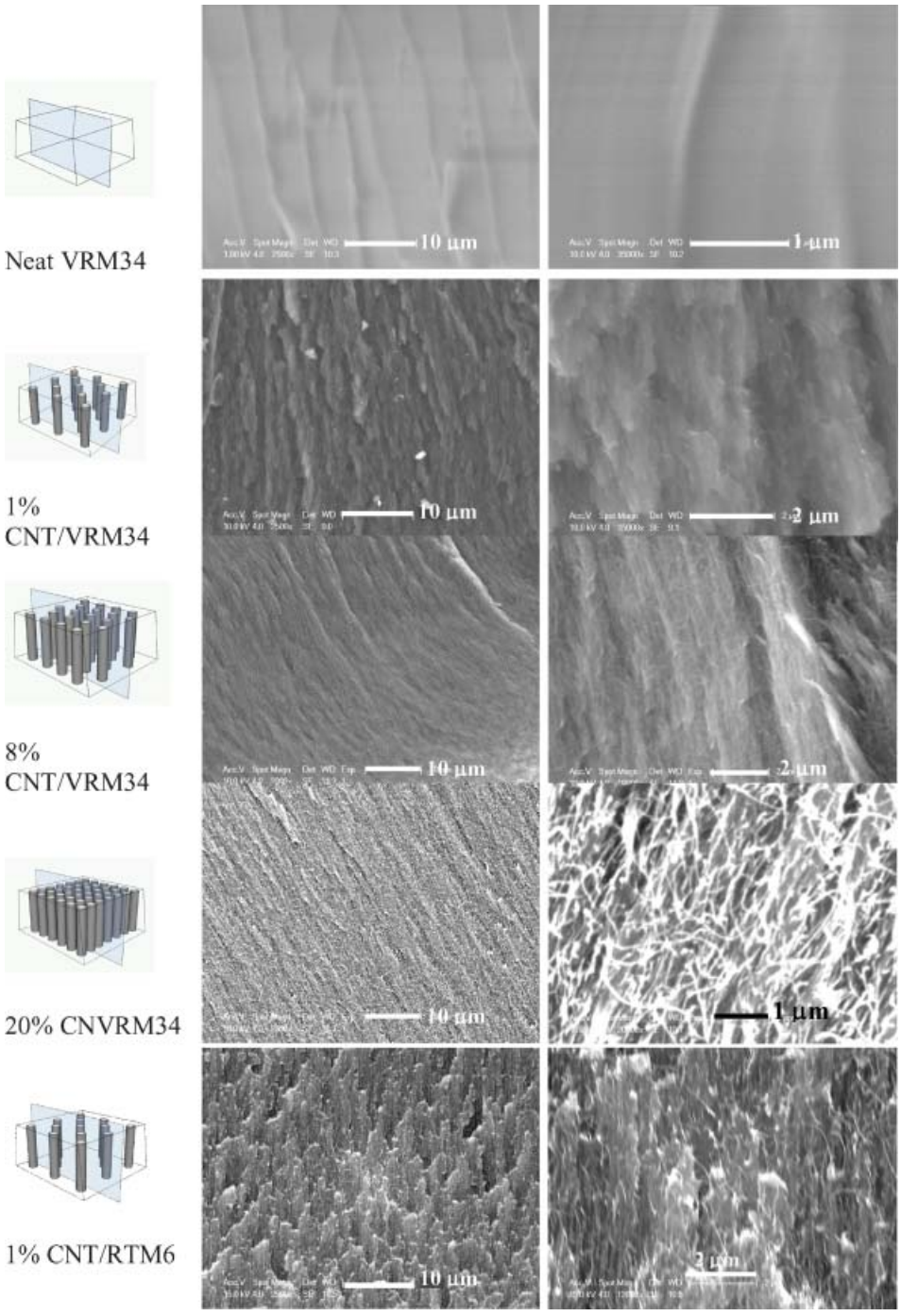

Figure 3. Fracture surfaces of A-CNT nanocomposites. Evolution of fracture surface as volume fraction is increased for VRM34 epoxy, and 1% RTM6 A-CNT nanocomposite.

yielding close to no net volume change between the CNT forest and the NC. Conversely, at low volume fractions, the compaction forces can split the forest and create regions that are filled by the infusing polymer, consistent with observations.

It is also of interest to determine the length of CNTs (forest height) that can be wet by a given polymer. This length has practical importance for several hybrid advanced composite architectures being developed,[36,37] as capillarity-driven wetting is used to pull the polymers into forests of CNTs placed on or between advanced micrometer-diameter. fibers of traditional laminated composites. Viscosity primarily dictates this length.[20] For the epoxies studied here, with viscosities in the range of 8–33 cP, 1% volume fraction A-CNT forests were fully wet to heights exceeding 1 mm.

Several groups have investigated capillarity-induced wetting of CNT forests, focused on increasing the volume fraction of a

dry CNT forest using solvent-induced densification, or creating controlled CNT micropatterns.[32,33,38,39] Low-viscosity and low-boiling-point solvents (e.g., isopropyl alcohol) are introduced into the ends of a CNT forest and because of capillary forces, the solvent is pulled into the forest and at the same time densifies it, creating a higher-volume-fraction A-CNT forest. The solvent-induced densification approach does not provide control over volume fraction, and the final densified forest is a function of the solvent and forest. In some cases large (and controlled, or patterned) cellular structures are formed in the A-CNT forest. In other cases, CNT forest microfeatures (e.g., a pillar of square cross-section) having aspect ratios close to 1 are densified by the solvent to create higher-volume-fraction microfeatures.[31,40] Capillarity-driven patterning is well reviewed[32,41,42] and the degree of wetting and densification are noted to be a function of the contact (or wetting) angle of the liquid with the CNTs, the liquid's viscosity, and CNT characteristics (diameter, volume fraction). Solvent-induced densification was also explored in this work using isopropyl alcohol, and the resulting forests were highly contracted, irregular, and contained micrometer-scale cells as observed by others. Such structures were considered unsuitable for creating homogeneous A-CNT NCs. A hybrid technique combining mechanically and solvent-induced densification reveals that moderately (mechanically) densified forests can be further densified, uniformly, using solvents. A-CNT forests were mechanically densified to ca. 10%, further densified with isopropyl alcohol to ca. 20%, and then wet with resin to make a NC. The results were equivalent (no voids or polymer-rich regions, aligned CNTs, etc.) to a 20% mechanical densification and polymer infusion process.

NC cross-sections were also inspected under transmission electron microscopy (TEM). TEM samples were prepared using focused-ion beam (FIB) and imaged with a JEOL TEM2011. Mechanical polishing and cryogenic microtome were not successful in creating TEM samples. A TEM of an 8% CNT V_f A-CNT NC is shown in Figure 4. CNT wall structure is clearly evident inside the epoxy matrix, as is CNT alignment. At this volume fraction, the average CNT spacing should be ca. 20 nm, which is confirmed by TEM. It is not possible to discern whether polymer is inside the CNTs or not. Alignment of the CNTs within the NCs is also evaluated using small-angle X-ray scattering (SAXS). SAXS reveals that the aligned morphology of a CNT forest is maintained after the process steps (densification, wetting, and curing) to form an A-CNT NC. A typical SAXS image of an A-CNT NC sample is shown in Figure 5, showing a characteristic asymmetric pattern of aligned structures. Alignment is quantified using the Hermans orientation parameter (f), which is calculated from an azimuthal scan of the scattered intensity at the location of the peak corresponding to the CNT form factor.[43] Limiting values of $f = 1$, 0, and $-\frac{1}{2}$ correspond to perfect vertical alignment, random orientation, and perfect horizontal alignment, respectively. The Hermans orientation parameter for the A-CNT NCs varies from 0.4–0.5, which is close to the value of 0.6–0.7 measured for as-grown (1% volume fraction, undensified) CNT forests. The small decrease in the orientation parameter could be in part due to the scattering contribution from the unoriented polymer.

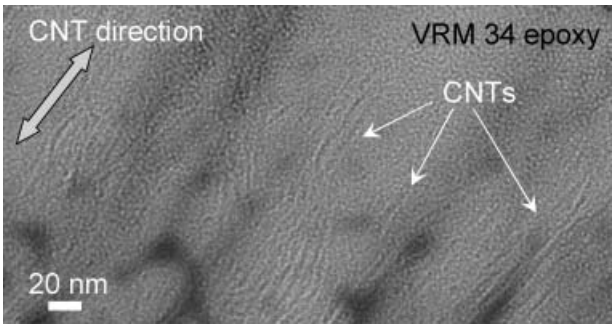

Figure 4. TEM image of aligned-CNT-nanocomposite cross-section revealing CNT wall structure embedded in the epoxy (VRM34 at 8% V_f).

Interfacial interactions play a key role in describing the mechanical and transport behavior of composites,[44] and the role of the interface is more pronounced for NCs because the interfacial area is at least one order magnitude higher than traditional composites. Furthermore, the polymer interacts with the highly curved surface of the CNT, which is on the order of the radius of gyration (ca. 3–30 nm) for polymers.[45] Polymers near the surface of a nanostructure behave differently than those in the bulk,[46,47] causing variations in the degree of cure, chain mobility, and chain conformation or crystallinity in the region near the nanostructure. The size of this modified region near the nanostructure, usually called the interphase region, can be between 10–100 nm from the surface.[46] Thus, the existence of nanostructures during polymerization has been shown to induce polymer morphology changes, particularly crystallization, in several thermoplastics. The nanostructures are thought to act as templates for the polymer to crystallize around, and the effect on glass transition temperature is usually measured,[48] and the effect on mechanical properties can be significant.[49,50]

In the A-CNT NCs considered here, the capillarity-driven wetting and the aligned nature of the CNTs can cause polymer packing and may induce polymer changes as well. Indeed, at high volume fractions and for small-diameter CNTs as used in this work, inter-CNT spacing can approach the values of the interphase region and the radius of gyration of polymers as shown in Figure 6. Considering the size of the interphase on the order of 10–100 nm, up to 100% of the polymer volume fraction

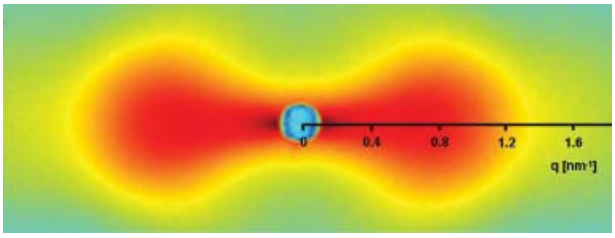

Figure 5. Characteristic SAXS pattern of A-CNT NCs (1% CNTs in VRM34) indicating vertical alignment of CNTs within the matrix.

ADVANCED MATERIALS

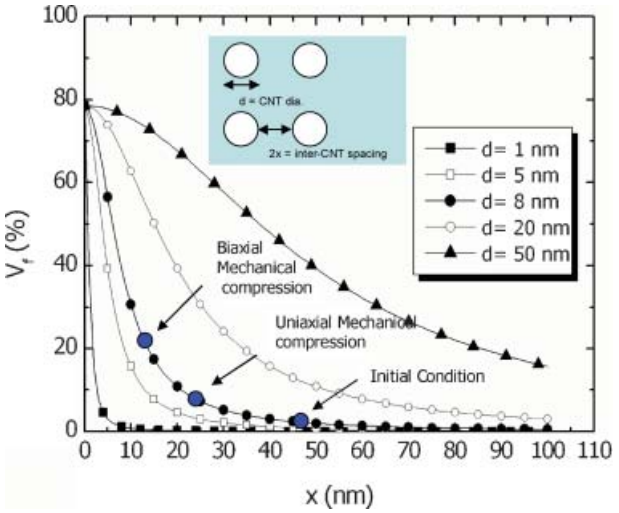

Figure 6. Trend of VACNT-NC volume fraction for different diameter CNTs.

would be interphase, and if a distance equal to the polymer radius of gyration is needed between adjacent CNTs, then high volume fractions are difficult to achieve for small dia. CNTs (e.g., our 8 nm CNTs with $x = 10$ nm have a maximum volume fraction of ca. 30%). Thermoplastics are generally known to be more susceptible to crystallization effects of additives than thermosets, however, this has not been explored to our knowledge. Here we use wide-angle X-ray scattering (WAXS) to interrogate A-CNT NCs with regard to changes in the polymer induced by the CNTs.

Wide-angle X-ray scattering was performed using the same setup as SAXS yet with a much shorter sample-detector distance for capturing a wider scattering angle. WAXS therefore examines features on the sub-nanometer scale ($q = 2\pi/d$). WAXS data for a pure A-CNT forest, pure VRM34 thermoset, and A-CNT NCs with $V_f = 1\%$, 2%, and 4% are shown in Figure 7. The integrated intensity ($\pm 10^\circ$ from horizontal) profiles reveal two distinct peaks; the peak at $q = 14.2$ nm^{-1} in the pure VRM34 sample (see arrow on pure VRM34 plot in Fig. 7) indicative of local packing among polymer chains, and the peak at 19.2 nm^{-1} in the as-grown CNT forest sample (see arrow on pure MWNT plot in Fig. 7) represents the CNT interlayer spacing ($d = 0.34$ nm). There is no indication of any induced crystallinity or preferential orientation of the polymer due to the addition of the CNTs. Similar behavior is observed for all other thermoset composites considered here. The CNT and polymer peaks are convoluted at low V_f, and scattering from the CNT walls dominates the intensity at higher volume fractions.

The morphology and alignment of high-volume fraction A-CNT NCs has been presented for advanced thermoset epoxy polymers demonstrating that variable volume fractions are achievable using the mechanical densification and capillarity-driven wetting approach. Alignment of the CNTs is confirmed via TEM and SAXS imaging. Such specimens will be useful in experimentally evaluating mechanical and other physical engineering properties of such materials (e.g., stiffness, strength, resistivity, thermal conductivity) and should also be useful in identifying and evaluating nanoscale interaction effects and how they evolve with high fractions (and close packing) of aligned CNTs. Of particular interest in both cases is nonisotropic physical behavior, such as stiffness along the CNT axes versus transverse to them. The base-growth CNT growth mechanism used herein is especially advantageous in creating homogeneous NCs for such studies, due to the lack of catalyst

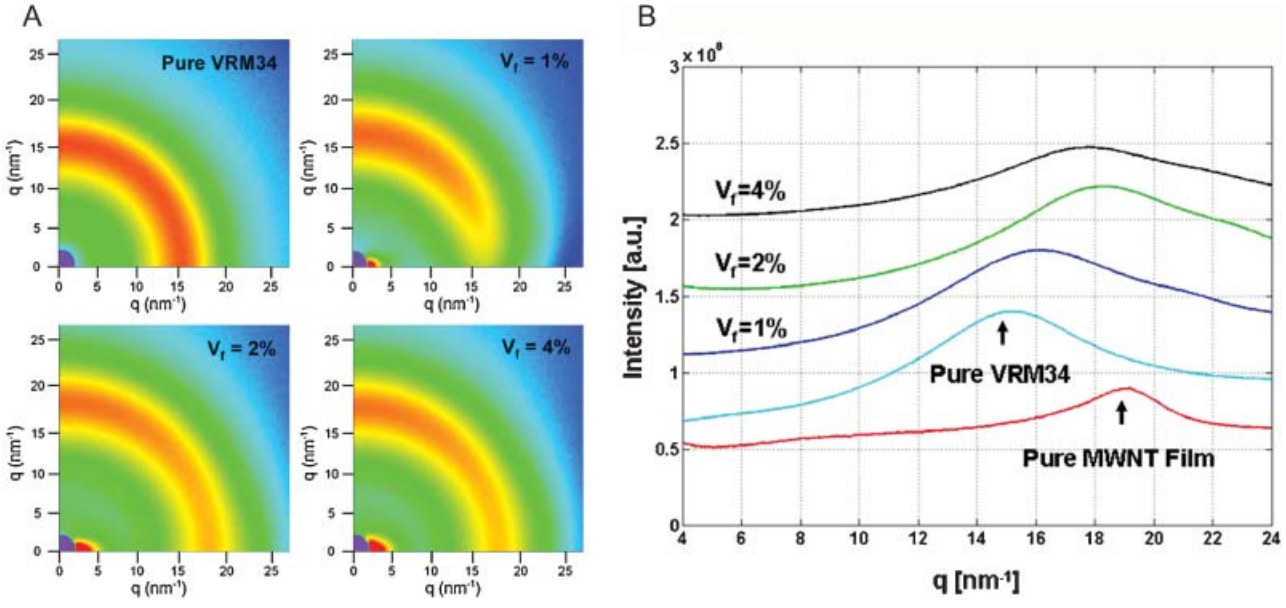

Figure 7. WAXS analysis of VRM34 A-CNT NCs. A) Images showing azimuthally symmetric scattering which indicates there is no significant polymer crystallinity in the samples. B) Integrated intensity profiles ($\pm 10^\circ$ from *x*-axis), showing presence of distinct peaks for polymer chain packing and CNT wall-wall spacing.

Table 1. Thermoset epoxy characteristics.

Epoxy	Manufacturer	Usual application	Temperature during wetting [°C]	Viscosity at wetting temp. [cP]	Cure cycle
VRM34	Hexcel	Aerospace-grade advanced composites	90	12	1 h/160 °C 3 h/180 °C
RTM6	Hexcel	Aerospace-grade advanced composites	90	33	1 h/160 °C 3 h/180 °C
SU-8 2002	MicroChem	Microfabrication	65	8	Prebake: 5 min/60 °C Exposure: UV light for 1 min Postbake: 5 min/90 °C Hardbake: 30 min/130 °C

particles in the interior of the samples as would be found with floating-catalyst CNT synthesis. The finding of epoxy infusion into the aligned CNT forests, even at high CNT volume fractions, suggests a mechanism by which hybrid advanced composites containing aligned CNTs can be fabricated. An upper limit of CNT volume fraction that can be wet by polymers has not yet been identified: wetting is effective to greater than 20% CNT volume fraction when the MWNTs are ca. 8 nm in diameter. It is likely that wetting of similar volume fraction single-wall CNTs may have quite different characteristics due to bundling/roping of SWNTs. Polymer packing and crystallization effects due to the CNTs, even at high CNT volume fractions, are not observed and may suggest that existing advanced thermosets can be combined effectively with CNTs without CNT functionalization or polymer modification. Such millimeter-scale A-CNT NC samples should provide an effective experimental platform for studying topics such as CNT functionalization, polymer modification, interphase formation due to the CNTs, and other processing effects such as microwave bonding.[51] Future studies will address the mechanical and multifunctional properties of the high-volume-fraction A-CNT NCs, including similar characterizations using thermoplastics. Ultrahigh-volume-fraction A-CNT NCs have potential for numerous applications, somewhat famously as a material necessary to realize the so-called ''space elevator''. Certainly, such millimeter-scale NCs currently demonstrated are of interest in applications where managing electrical and thermal conductivities[52] is required.

Experimental

Aligned-CNT Nanocomposite Preparation and Characterization: Aligned nanotubes applied in this work were grown by CVD methods on a silicon substrate with catalyst deposited on it by an e-beam method. In this process, ethylene was used as the precursor and iron as catalyst. CNT forests were grown on $1 \times 1\,cm^2$ square Si substrates. As-grown CNT forests could be extracted easily from the substrate using a standard lab razor blade. After separation, nanotubes were held together by physical entanglement and van der Waals forces in such a way that the forest could be handled as a film. A-CNT NCs were formed following the process described in the main text (see Fig. 1A) and characterized primarily with SEM using JEOL 5910 and XL 30 instruments. The resolutions of these microscopes are 1 μm and 50 nm, respectively.

Thermoset Epoxy Properties: Characteristics of the thermosetting epoxies used in this work are given in Table 1. All epoxies were utilized following the manufacturer's recommended curing cycle. The advanced composite epoxies were used at elevated temperature, as they would be during resin transfer moulding (RTM) processing of advanced composites. SU-8 is processed following standard microfabrication procedures used to create microstructures (exposure to UV light, which when combined with patterning allows polymer microstructures to be formed). Since regular light contains UV rays in its spectrum, it was necessary to work with this epoxy in a UV-free room. In this manner, all experiments done with SU-8 were performed at the Fabrication Lab from Microsystem Technology Laboratories (MTL/MIT).

X-ray Scattering: X-ray studies were performed at the G1 beamline station at the Cornell High Energy Synchrotron Source (CHESS). The wavelength of the X-rays was 0.1239 nm, and the sample to detector distance was calibrated with silver behenate (first order scattering vector q of $1.076\,nm^{-1}$, with $q = 4\pi \sin(\theta/\lambda)$, where 2θ is the scattering angle and λ is the wavelength). Slit collimation was used to achieve a resulting beam spot that was approximately 0.2 mm in height and 0.4 mm in width (the y- and x-axes, respectively). A slow-scan CCD-based X-ray detector, home-built by Dr. M. W. Tate and Dr. S. M. Gruner of the Cornell University Physics Department, was used for data collection.

Received: January 30, 2008
Revised: March 24, 2008
Published online:

[1] S. Iijima, *Nature* **1991**, *354*, 56.
[2] A. Oberlin, M. Endo, T. Koyama, *J. Cryst. Growth* **1976**, *32*, 335.
[3] M. S. Dresselhaus, G. Dresselhaus, P. C. Eklund, *Science of Fullerenes and Carbon Nanotubes: Their Properties and Applications*, Academic, San Diego. CA **1996**.
[4] M. S. Dresselhaus, A. Jorio, A. G. Souza Filho, G. Dresselhaus, R. Saito, *Phys. B* **2002**, *323*, 15.
[5] P. M. Ajayan, J. M. Tour, *Nature* **2007**, *447*, 1066.
[6] K. Schulte, A. H. Windle, *Compos. Sci. Technol.* **2007**, *67*, 777.
[7] E. T. Thostenson, Z. Ren, T.-W. Chou, *Compos. Sci. Technol.* **2001**, *61*, 1899.
[8] E. T. Thostenson, C. Li, T.-W. Chou, *Compos. Sci. Technol.* **2005**, *65*, 491.
[9] R. A. Vaia, H. D. Wagner, *Mater. Today* **2004**, *32*.
[10] T. Tong, Y. Zhao, L. Delzeit, A. Kashani, M. Meyyappan, *IEEE Trans. Compon Packag. Technol.* **2007**, *30*.
[11] A. H. Windle, *Compos. Sci. Technol.* **2007**, *67*, 929.
[12] J. N. Coleman, M. Cadek, K. P. Ryan, A. Fonseca, J. B. Nagy, W. J. Blau, M. S. Ferreira, *Polymer* **2006**, *47*, 8556.
[13] Y. L. Li, I. A. Kinloch, A. H. Windle, *Science* **2004**, *304*, 276.
[14] R. Guzmán de Villoria, A. Miravete, J. Cuartero, A. Chiminelli, N. Tolosana, *Composites Part B* **2006**, *37*, 273.
[15] P. Labordé-Lahoz, W. Maser, T. Martínez, A. Benito, T. Seeger, P. Cano, R. Guzmán de Villoria, A. Miravete, *Mech. Adv. Mater. Struct.* **2005**, *12*, 13.

[16] M. Zhang, K. R. Atkinson, R. H. Baughman, *Science* **2004**, *306*, 1358.
[17] L. M. Ericson, H. Fan, H. Peng, V. A. Davis, W. Zhou, J. Sulpizio, Y. Wang, R. Booker, J. Vavro, C. Guthy, A. N. G. Parra-Vasquez, M. J. Kim, S. Ramesh, R. K. Saini, C. Kittrell, G. Lavin, H. Schmidt, W. W. Adams, W. E. Billups, M. Pasquali, W. Hwang, R. H. Hauge, J. E. Fischer, R. E. Smalley, *Science* **2004**, *305*, 1447.
[18] P. Miaudet, S. Badaire, M. Maugey, A. Derre, V. Pichot, P. Launois, *Nano Lett.* **2005**, *5*, 2212.
[19] A. B. Dalton, S. Collins, J. Razal, E. Munoz, V. H. Ebron, B. G. Kim, J. N. Coleman, J. P. Ferraris, R. H. Baughman, *J. Mater. Chem.* **2004**, *14*, 1.
[20] W. Fang, H. Y. Chu, W. K. Hsu, T. W. Cheng, N. H. Tai, *Adv. Mater.* **2005**, *17*, 2987.
[21] N. R. Raravikar, L. S. Schadler, A. Vijayaraghavan, Y. Zhao, B. Wei, P. M. Ajayan, *Chem. Mater.* **2005**, *17*, 974.
[22] B. J. Hinds, N. Chopra, T. Rantell, R. Andrews, V. Gavalas, L. G. Bachas, *Science* **2004**, *303*, 62.
[23] L.-Q. Liu, D. Tasis, M. Prato, H. D. Wagner, *Adv. Mater.* **2007**, *19*, 1228.
[24] Y. Dror, W. Salalha, W. Pyckhout-Hintzen, A. L. Yarin, E. Zussman, Y. Cohen, *Prog. Colloid Polym. Sci.* **2005**, *130*, 64.
[25] W. Salalha, Y. Dror, R. L. Khalfin, Y. Cohen, A. L. Yarin, E. Zussman, *Langmuir* **2004**, *20*, 9852.
[26] B. Vigolo, A. Penicaud, C. Coulon, C. Sauder, R. Pailler, C. Journet. *Science* **2000**, *290*, 1331.
[27] P. Podsiadlo, A. K. Kaushik, E. M. Arruda, A. M. Waas, B. S. Shim, J. Xu, H. Nandivada, B. G. Pumplin, J. Lahann, A. Ramamoorthy, N. A. Kotov, *Science* **2007**, *318*, 80.
[28] B. S. Shim, Z. Y. Tang, M. P. Morabito, *Chem. Mater.* **2007**, *19*, 5467.
[29] A. J. Hart, A. H. Slocum, *J. Phys. Chem. B* **2006**, *110*, 8250.
[30] A. J. Hart, A. H. Slocum, *Nano Lett.* **2006**, *6*, 1254.
[31] E. J. García, A. J. Hart, B. L. Wardle, A. H. Slocum, *Nanotechnology* **2007**, *18*, 165602.
[32] X. Huang, Z. J. Zhou, E. Sansom, M. Gharib, S. C. Haur, *Nanotechnology* **2007**, *18*, 305301.
[33] H. Liu, J. Zhai, L. Jiang, *Soft Matter* **2006**, *2*, 811.
[34] R. Guzman de Villoria, A. Miravete, *Acta Mater.* **2007**, *55*, 3025.
[35] R. Guzman de Villoria, *Ph. D. Thesis*, University of Zaragoza, Spain **2007**.
[36] E. García, J. Hart, B. L. Wardle, A. Slocum, D. J. Shim, presented at the *Proc. of the 16th Int. Conf. on Composite Materials (ICCM)*, Kyoto, Japan, July 8–13, **2007**.
[37] N. Yamamoto, E. Garcia, J. Hart, B. L. Wardle, A. Slocum, presented at the *Proc. of the 16th Int. Conf. on Composite Materials (ICCM)*, Kyoto, Japan, July 8–13, **2007**.
[38] D. N. Futaba, K. Hata, T. Yamada, T. Hiraoka, Y. Hayamizu, Y. Kakudate, O. Tanaike, H. Hatori, M. Yumura, S. Iijima, *Nat. Mater.* **2006**, *5*, 987.
[39] N. Chakrapani, B. Wei, A. Carrillo, P. M. Ajayan, R. S. Kane, presented at the *Proc. of the Natl. Acad. Sci. USA*. **2004**, *101*.
[40] E. J. García, A. J. Hart, B. L. Wardle, A. H. Slocum, *Adv. Mater.* **2007**, *19*, 2151.
[41] E. Dujardin, T. W. Ebbesen, H. Hiura, K. Tanigaki, *Science* **1994**, *265*, 1850.
[42] A. V. Bazilevsky, K. Sun, A. L. Yarin, C. M. Megaridis, *Langmuir* **2007**, *23*, 7451.
[43] B. N. Wang, R. D. Bennett, E. Verploegen, A. J. Hart, R. E. Cohen, *J. Phys. Chem. C* **2007**, *111*, 5859.
[44] R. E. Gorga, K. K. S. Lau, K. K. Gleason, R. E. Cohen, *J. Appl. Polym. Sci.* **2006**, *102*, 1413.
[45] K. I. Winey, R. A. Vaia, *MRS Bull.* **2007**, *32*, 314.
[46] P. Ajayan, P. Braun, L. Schadler, *Nanocomposite Science and Technology,* Wiley-VCH, Weinheim. Germany **2003**.
[47] A. H. Barber, S. R. Cohen, H. D. Wagner, *Appl. Phys. Lett.* **2003**, *82*, 4140.
[48] L. S. Schadler, S. K. Kumar, B. C. Benicewicz, S. L. Lewis, S. E. Harton, *MRS Bull.* **2007**, *32*.
[49] J. N. Coleman, M. Cadek, R. Blake, V. Nicolosi, K. P. Ryan, C. Belton, A. Fonseca, J. B. Nagy, K. Gun'ko, W. J. Blau, *Adv. Funct. Mater.* **2004**, *14*, 791.
[50] K. P. Ryan, M. Cadek, V. Nicolosi, S. Walker, M. Ruether, A. Fonseca, J. B. Nagy, W. J. Blau, J. N. Coleman, *Synth. Met.* **2006**, *156*, 332.
[51] C. Y. Wang, T. H. Chen, S. C. Chang, S. Y. Cheng, T. S. Chin, *Adv. Funct. Mater.* **2007**, *17*(12), 1979.
[52] H. M. Duong, D. V. Papavassiliou, K. J. Mullen, S. Maruyama, *Nanotechnology* **2008**, *19*, 065702.

